

Thermophysical and Optical Properties of Materials Considered for use on the LDSD Test Vehicle

Matthew Redmond¹ and A.J. Mastropietro¹

NASA Jet Propulsion Laboratory, California Institute of Technology, Pasadena, CA, 91109

In June 2014, the first of multiple flights in the Low Density Supersonic Decelerator (LDSD) technology development program took place and successfully demonstrated a Supersonic Inflatable Aerodynamic Decelerator (SIAD) in Mars-like conditions. Although the primary goal of the technology program was the development of new decelerators for landing heavier payloads on Mars, the low-cost thermal design of the test vehicle was only possible through the innovative use of a combination of both commercial off the shelf (COTS) and aerospace grade materials. As a result, numerous thermophysical and optical property measurements were undertaken to characterize material candidates before the final material selection was made. This paper presents thermophysical and optical property measurements performed over the course of the LDSD test vehicle development, including those not ultimately selected for use on the vehicle. These properties are compared and contrasted with the existing measurements available in previous literature.

Nomenclature

A	= Area
c_p	= Specific heat
k	= Thermal conductivity
Q	= Power dissipation
α	= Thermal diffusivity
ΔT	= Temperature difference
ρ	= Density
ASTM	= American Society for Testing and Materials
BLDT	= Balloon Launch Decelerator Test
COTS	= Commercial Off The Shelf
DSC	= Differential Scanning Calorimetry
LDSD	= Low Density Supersonic Decelerator
MDSC	= Modulated Differential Scanning Calorimetry
SIAD	= Supersonic Inflatable Aerodynamic Decelerator
SSDS	= Supersonic Disk Sail
TESA	= Thermal Emissivity Solar Absorptivity

I. Introduction

PREVIOUS lander missions to Mars have all relied on heritage landing technology developed for the Viking program in the 1970s and tested on balloon launched decelerator test vehicles (BLDT)¹⁻³. However, future missions to Mars will require new types of decelerator systems in order to land heavier payloads at higher altitudes. Although many different types of decelerator systems have been studied over the past 50 years⁴ NASA's Low Density Supersonic Decelerator (LDSD) program has been tasked with developing and testing three new decelerator technologies to enable future missions, shown in Figure 1. One of these, the Supersonic Disk Sail (SSDS) parachute is similar to the Disk-Gap-Band parachute tested during the BLDT program. The other two are Supersonic Inflatable Aerodynamic Decelerator (SIAD) devices. The SIAD-R is a 6 meter outside diameter torus intended for robotic missions which inflates using compressed gas. The SIAD-E is an 8 meter outside diameter isotenoid intended for

¹ Thermal Engineer, Thermal Technology and Fluid Systems

human exploration missions which inflates using a combination of compressed gas and ram air. Details on the development of the parachute, SIADs, and test vehicle can be found in⁵⁻⁹.

The first of the test flights successfully took place in June 2014, with additional flights scheduled for the summers of 2015 and 2016. The flight profile of the vehicle is summarized in Figure 2. The test vehicle is launched using a helium filled balloon provided by Columbia Scientific Balloon Facility. When it reaches a float altitude of approximately 118,000 ft (~36 km), the test vehicle is dropped, spin stabilized using spin up motors, and a large solid rocket motor fires to accelerate the test vehicle to around Mach 4. Once the main motor burn is finished, the test vehicle is despun, and the test period begins. The SIAD is tested first, followed by a test of the SSDS parachute, and concluding with a descent into the ocean and subsequent recovery. The flight spans a number of environmental regimes including ascent, float, test, and descent which can be challenging from a thermal perspective. As a result, various types of insulation have been successfully used for thermal management in both the LDSD test vehicle and the previous Viking-era BLDT test¹⁰⁻¹³.

During the LDSD test vehicle design, there was a strong desire to keep costs down since the primary goal of the test program was technology development. As a result, both commercial off the shelf (COTS) and aerospace grade materials were considered for use in the LDSD test vehicle thermal design. However, it was necessary to characterize both the thermophysical and optical properties of the materials under consideration before a final design choice was made. Measurements of thermal emissivity, solar absorptivity, specific heat, and thermal conductivity were made over the course of LDSD test vehicle development.

These measurements were performed alike for materials used on the test vehicle, as well as for materials which were ultimately not used on the test vehicle for various reasons. This work presents a summary of the material property measurements taken in the LDSD test program.

In this work, materials are described in as much detail as possible, but it is inevitable that some of these materials will change trade names in the future. As a result, a comprehensive (but not exhaustive) collage of the materials described in this paper is contained in Figure 3.

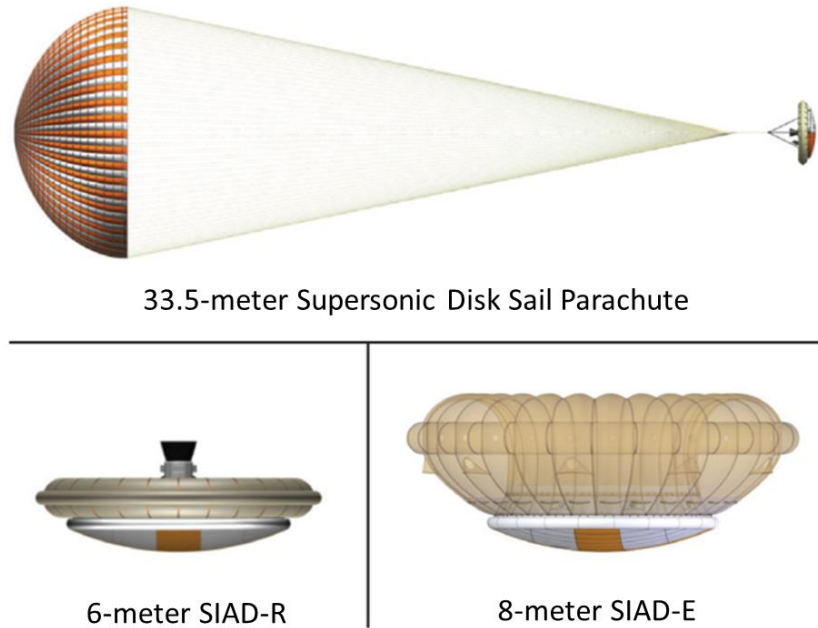


Figure 1. Technologies tested in the LDSD test program⁸.

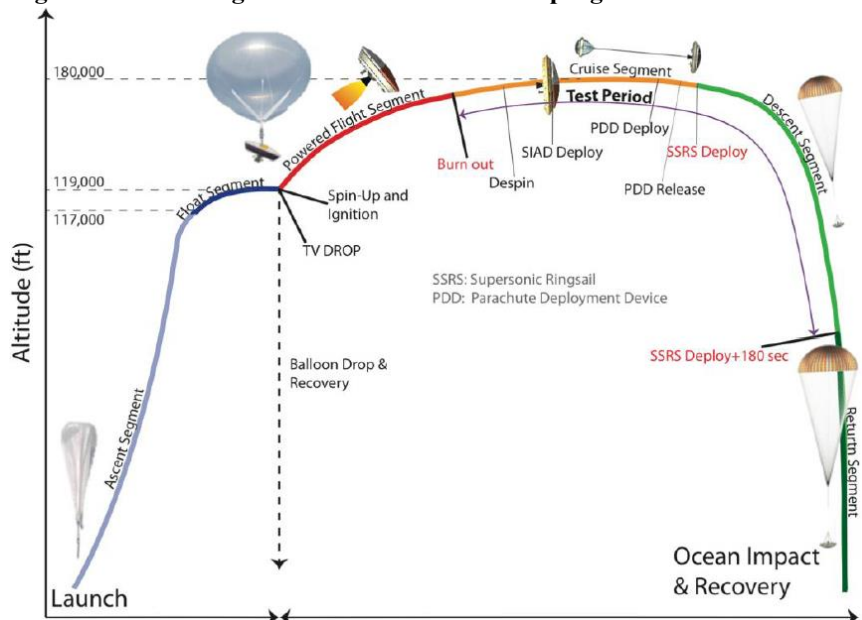


Figure 2. Summary of the flight profile⁹.

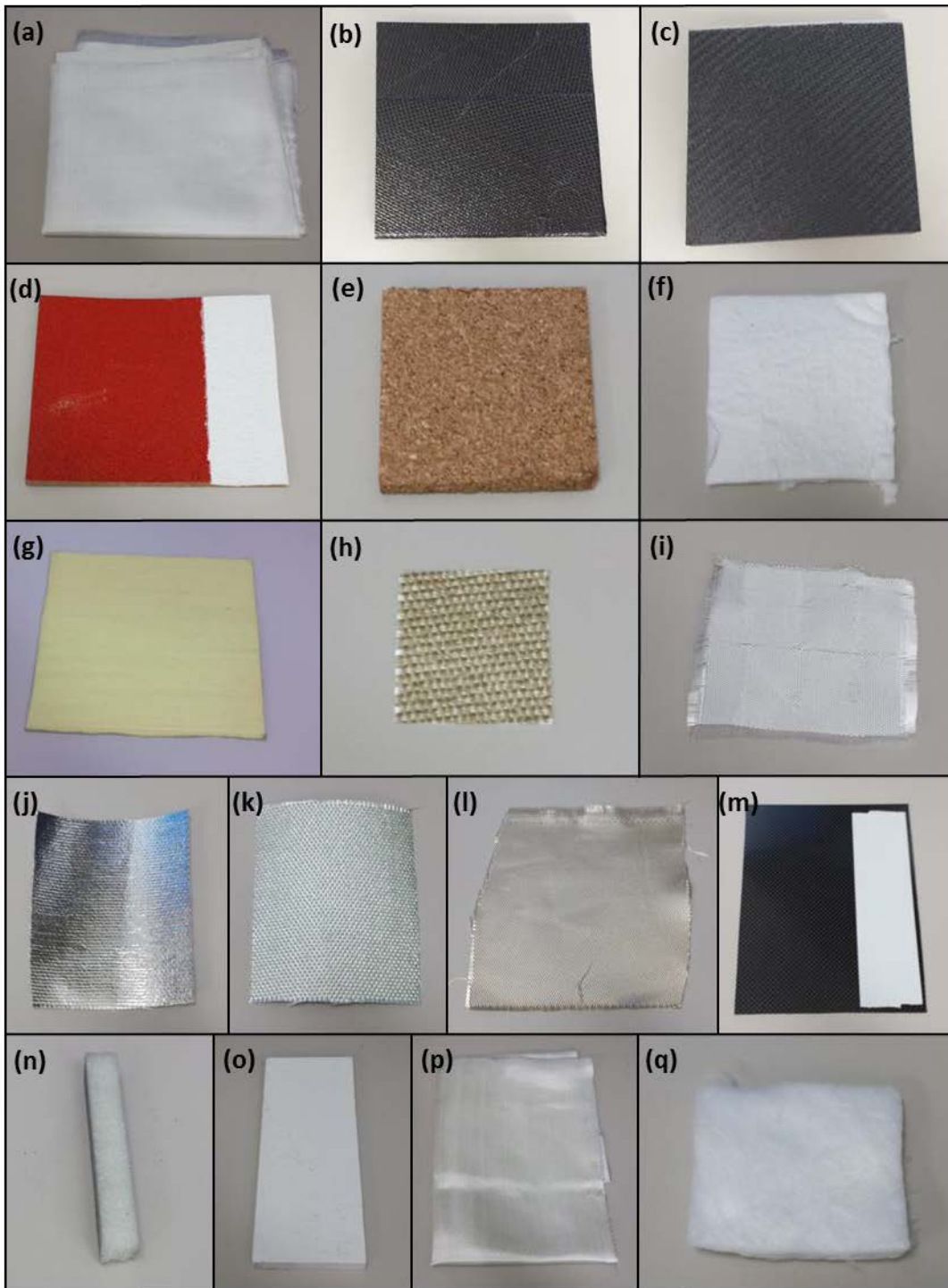


Figure 3. Collage of various materials described in this paper. (a) BGF Industries Plain Untreated Fiberglass Fabric, Style 7628 (b) Carbon Composite (c) Carbon Composite, Sanded (d) Cork, 1 Coat of Orange Paint / 3 Coats of White Zynolyte® HiTemp Paint (e) Cork, Bare (f) Fiberfrax® Ceramic Fiber Paper, 970-K (g) Kevlar® Felt (h) Newtex ZetexPlus® A-400 Vermiculite Coated Glass Fabric (i) Newtex Z-Fil™ F-401 Filament Glass Fabric (j) Newtex Z-Flex® A-302 Aluminumized Fabric (Aluminum side) (k) Newtex Z-Flex® A-302 Aluminumized Fabric (Fabric side) (l) Newtex Z-Sil™ F-605 Silica Fabric (m) Polyken® 223 White Duct Tape on Carbon Composite (n) Rohacell® Foam (110 Kg/m³) (o) SuperFiretemp® Calcium Silicate Insulation (p) Thermostatic Industries S-2 Glass Cloth (q) ZIRCAR™ Alumina Mat

II. Optical Properties

Most of the optical property measurements were taken at JPL using the TESA 2000 in ambient conditions. The TESA 2000 measures the total hemispheric reflectance of a surface over a variety of wavelengths. The reflectance measurements are either integrated over the 250 to 2500 nm range in order to determine the solar absorptivity or integrated over the 3 to 35 μm range in order to determine the thermal emissivity of a material. Prior to and after each use, the TESA 2000 calibration was verified against low and high thermal emissivity and solar absorptivity calibration coupons to a value within 0.05. The measurement uncertainty of the TESA 2000 is listed +/- 1% for gray and +/- 3% for non-grey samples¹⁴. Some optical property measurements were also contracted out to AZ Technology. The integrated hemispherical thermal emissivity and solar absorptivity of the materials measured are shown in Table 1.

Table 1: Integrated hemispherical thermal emissivity and solar absorptivity of measured surface coatings and bare materials.

Material	Thermal Emissivity	Solar Absorptivity
BGF Industries Plain Untreated Fiberglass Fabric, Style 7628	0.85	0.31
Carbon Composite	0.83	0.91
Carbon Composite, Sanded	0.83	0.91
Cork, Bare	0.84	0.51
Cork, 1 Coat of Orange Paint	0.87	0.59
Cork, 1 Coat of White Zynolyte® HiTemp Paint	0.88	0.34
Cork, 2 Coats of White Zynolyte® HiTemp Paint	0.87	0.27
Cork, 3 Coats of White Zynolyte® HiTemp Paint	0.88	0.22
Cork, 4 Coats of White Zynolyte® HiTemp Paint	0.90	0.22
Fiberfrax® Ceramic Fiber Paper, 970-K	0.85	0.20
Newtex ZetexPlus® A-400 Vermiculite Coated Glass Fabric	0.81	0.48
Newtex Z-Fil™ F-401 Filament Glass Fabric	0.84	0.24
Newtex Z-Sil™ F-605 Silica Fabric	0.88	0.37
Newtex Z-Flex® A-302 Aluminized Fabric (Aluminum side)	0.05	0.11
Newtex Z-Flex® A-302 Aluminized Fabric (Fabric side)	0.87	0.34
Polyken® 223 White Duct Tape on Bare Aluminum	0.86	0.36
Polyken® 223 White Duct Tape on Carbon Composite	0.89	0.46
Polyken® 223 White Duct Tape, 4 Layers	0.88	0.33
Quartz Cyanate	0.89	0.81
Silicone Coated Kevlar (Kevlar Side)	0.85	0.47
Silicone Coated Kevlar (Silicone Side)	0.88	0.65
Thermostatic Industries S-2 Glass Cloth	0.85	0.22
Titanium, Grit Blasted	0.46 - 0.57	0.80 - 0.88
Titanium, 2 Coats of White Zynolyte® HiTemp Paint	0.87	0.29 - 0.32
Titanium, 2 Coats of White Zynolyte® HiTemp Paint after exposure to 700 °C steel block	0.83 - 0.87	0.29 - 0.46

One trend observed is that all the non-metallic surface coatings and materials had a thermal emissivity of between 0.8 and 0.9. However, the solar absorptivity of materials was more unpredictable. Although the solar absorptivity of a material can be conjectured by examining whether such a material seems “light” or “dark” to the naked eye, there were many times when “darker” materials had a lower measured solar absorptivity than “lighter”

materials. Some of the measured properties compare well to handbook and literature values while others do not. For example, the measured solar absorptivity (0.22 – 0.32) of white paint depends on the number of coats and on the substrate, but still compares well to the range of values for various white paints reported (0.1 – 0.4)^{15, 16}. Perhaps most importantly, the measured solar absorptivity of the orange paint was higher than expected based on handbook and literature values. The measured value of 0.59 actually is closer to the reported value for red colored surfaces (0.57) than for orange ones (0.51)^{15,16}. These trends highlight the importance of testing. Other interesting observations from these tests are noted below:

- The sanded and un-sanded carbon composite, although very different in appearance from one another, had identical thermal emissivity and solar absorptivity.
- A total of 3 coats of white paint on cork were necessary to lower the solar absorptivity to its minimum value. This is evident in the significant decrease in solar absorptivity of the painted cork between coats 1 and 2, and coats 2 and 3, compared to the insignificant decrease in solar absorptivity between coats 3 and 4.
- The Polyken® 223 white duct tape was partially transparent to at least some wavelengths in the solar spectrum. This is evident because of the different values for solar absorptivity of the tape on aluminum, carbon composite, or layered on itself. Multiple layers are necessary to achieve consistently “white” properties.
- Grit blasted titanium was found to have significantly variable solar absorptivity and thermal emissivity.
- Heating titanium coupons with 2 coats of White Zynolyte® HiTemp Paint using a 700 °C steel block resulted in no change or a slight decrease in thermal emissivity along with no change to a moderate increase in solar absorptivity. The heating of the coupons to the high temperature block was performed to see how thermal properties were affected by exposure to high temperatures using the following method. First, a steel block was placed in a high temperature oven and its temperature allowed to equilibrate. The block was then removed and placed onto the room temperature coupons, where a thermocouple measured the contact temperature between the block and the coupons.

III. Specific Heat

Most of the specific heat measurements were taken at Thermophysical Properties Research Laboratory, Inc. using a Differential Scanning Calorimeter (DSC) with sapphire as the reference material. These measurements were taken with an argon gas purge and a sample heating rate of 20 °C/min. The silicone coated Kevlar® specific heat measurements were taken at JPL using a Modulated Differential Scanning Calorimetry (MDSC) with sapphire as the reference material. These measurements were taken with a nitrogen gas purge and a sample heating rate of between 3 and 10 °C/min. The expected error was reported as < 1% for the measurements at JPL. All the specific heat measurements taken and reported meet the ASTM E1269 test standard¹⁷.

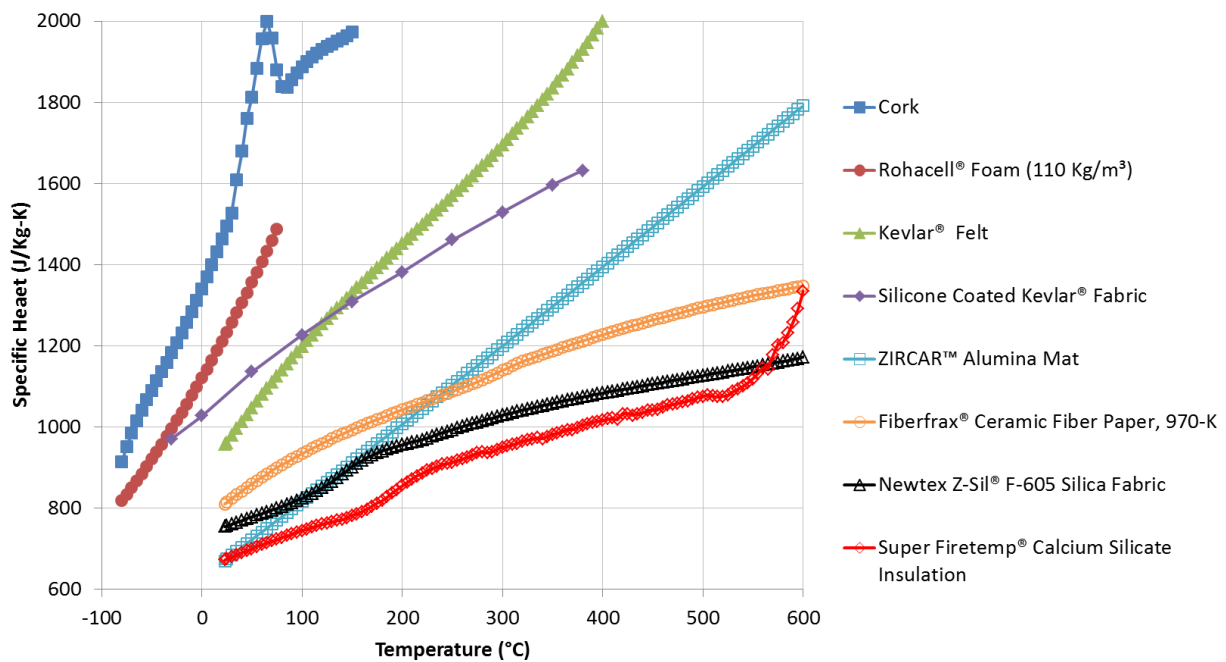


Figure 4. Measured values of specific heat as a function of temperature.

The specific heat of a variety of materials was measured over a range of temperatures, and the measured values are reported in Figure 4. The measured values are close to, but do not perfectly match the literature provided by the material manufacturers. Literature values for these materials are summarized in Table 2. The cork, ZIRCAR™ Alumina Mat, and Kevlar Felt literature values in Table 2 seem higher than the measured values in Figure 4. However, specific heat is often a less important parameter than the solar absorptivity, thermal emissivity, or thermal conductivity. Specific heat values do not affect steady state solutions, and the specific heat of a vast majority of materials varies by roughly one order of magnitude, while the thermal conductivity of materials varies by many orders of magnitude. In addition, uncertainties in specific heat can often be conservatively bounded by assuming a low value of specific heat, which results in more extreme transient temperature predictions. The same cannot always be said for thermal conductivity, thermal emissivity, or solar absorptivity, which often must be balanced so as to not be too large or too small. As a result, many of the specific heat values reported were obtained because they enabled transient measurements of thermal conductivity, which is the material property of primary importance. The local rise in specific heat of cork at around 80 °C is likely due to moisture evaporation or a chemical reaction.

Table 2: Specific heat measurements in the literature.

Material	Temperature (°C)	Specific Heat (J/Kg-K)
Cork ¹⁸	N/A	1800
Kevlar ^{® 19}	25	1420
Kevlar ^{® 19}	100	2010
Kevlar ^{® 19}	180	2515
ZIRCAR™ Alumina Mat ²⁰	N/A	1047

IV. Thermal Conductivity

Of all the measurements taken, the thermal conductivity measurement techniques were most varied due to the range of measurement needs and due to limitations of the different measurement techniques. A total of three measurement techniques were used to measure thermal conductivity: ASTM C177 (Guarded Hot Plate), ASTM E1461 (Laser Flash Diffusivity), and a non-standardized step heating technique.

The ASTM C177 thermal conductivity test method is a standardized test method used to measure the thermal conductivity of insulators (< ~ 16 W/m-K conductivity) in steady state²¹. In this test method, a guarded hot plate and two guard heaters are sandwiched between two planar specimens, as shown in Figure 5. The guard heaters are maintained within 0.1°C of the hot plate to ensure all heat generated by the hot plate travels through the tested materials. These components are placed between two cold plates with rubber pads to encourage good thermal contact, with secondary guard heaters and insulation placed around the assembly. The cold plates and hot plate are both instrumented with thermocouples and the hot plate power dissipation is adjusted until a temperature difference of 30 °C is maintained from the hot plate to the cold plates. The thermal conductivity of the sample is obtained using Fourier’s heat conduction equation, shown in Equation 1:

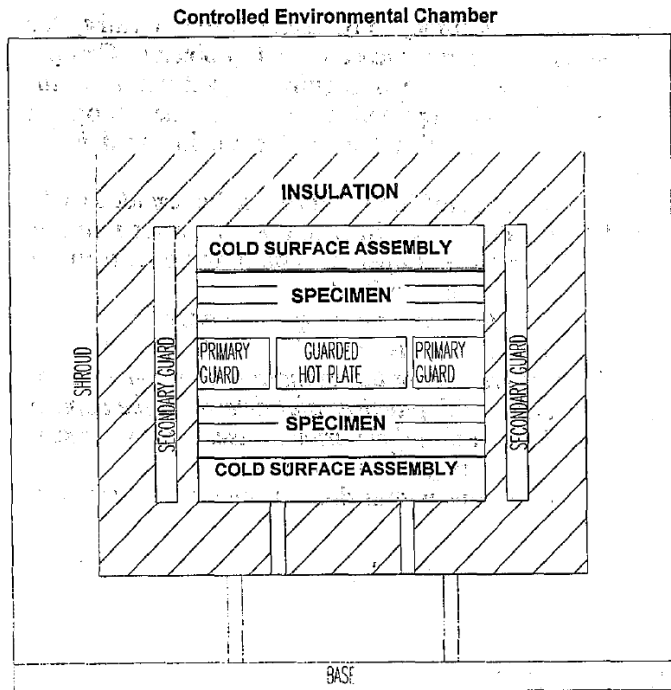


Figure 5. Schematic of ASTM C177 Test Apparatus²¹.

$$k = \frac{q}{\Delta T} \quad (1)$$

In this Equation, k is the thermal conductivity of the material, Q is the power which passes through the test coupon, A is the area normal to heat flux, and ΔT is the temperature difference between the hot and cold plates. The measurements performed to the ASTM C177 test standard were performed by Precision Measurement and Instruments Corporation.

The ASTM E1461 thermal conductivity test method is a standardized test method used to measure the thermal diffusivity of materials ranging from 0.1 to 1000 mm²/s using a transient technique²². In the laser flash diffusivity method, the front face of a small solid sample is exposed to a short laser burst while the temperature rise of the rear face is recorded. The temperature profile of the rear face as a function of time is then used to determine the thermal diffusivity of the sample. Once the thermal diffusivity, specific heat, and density of a material are known, its thermal conductivity can easily be calculated using Equation 2:

$$k = \alpha \rho c_p \quad (2)$$

In Equation 2, k is thermal conductivity, ρ is density, and c_p is specific heat. The measurements performed to the ASTM E1461 test standard were performed by Thermophysical Properties Research Laboratory, Inc.

The step heating method is similar to the ASTM E1461 laser flash diffusivity test method because it also is a transient method. In this method, a specimen is exposed to a uniform heat flux provided by a 600 Watt quartz-iodide tungsten element with an aluminum parabolic reflector. Temperature profiles of the sample, measured at three locations on the sample (one per face and one embedded within the sample), are used to calculate the thermal diffusivity of the measured material using a one-dimensional numerical analysis program. Once the thermal diffusivity of the measured material is known, Equation 2 can be used to calculate the thermal conductivity.

The thermal conductivity was measured for a large number of material candidates on the LDSO test vehicle because the thermal design of the test vehicle was very sensitive to the thermal conductivity of the insulators needed to protect the test vehicle against adverse thermal environments. The thermal conductivity of alumina mat as a function of temperature is shown in Figure 6. The measurements, taken at 1 torr of pressure, fall mostly in between the literature values reported for 760 torr (1 earth atmosphere) and 0 torr (vacuum). The thermal conductivity of Rohacell® at 760 torr (1 earth atmosphere) is shown in Figure 7 as a function of temperature. Measurements of Rohacell® taken with ASTM C177 had an unquantifiable degree of uncertainty due to a slight curvature in the material samples. As a result, additional measurements were performed with the step heating method. The measurements are in excellent agreement with each other and with literature values for 110 lb/ft³ (1762 Kg/m³) Rohacell®, giving a high degree of confidence in the measured values²³. The thermal conductivity of cork at 760 torr (1 earth atmosphere) was also measured using two different methods and is shown in Figure 8. Two measurements were taken for cork because it was found that the cork started to char and decompose at temperatures approaching 300 °C in the measurements taken with ASTM C177. As a result, secondary measurements were taken using the step heating method. The

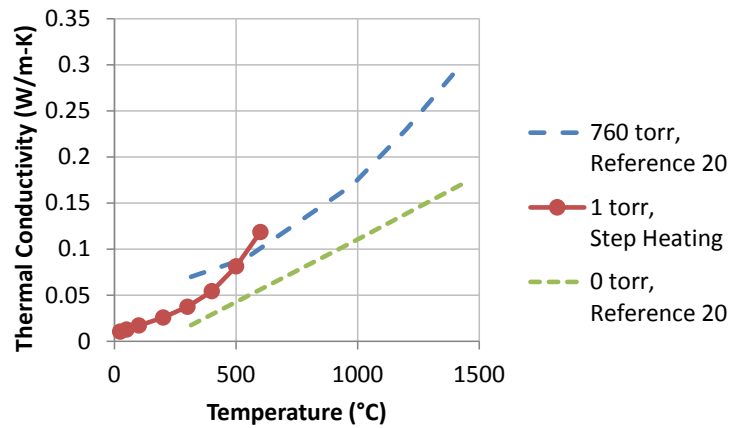


Figure 6. Thermal conductivity of alumina mat as a function of temperature.

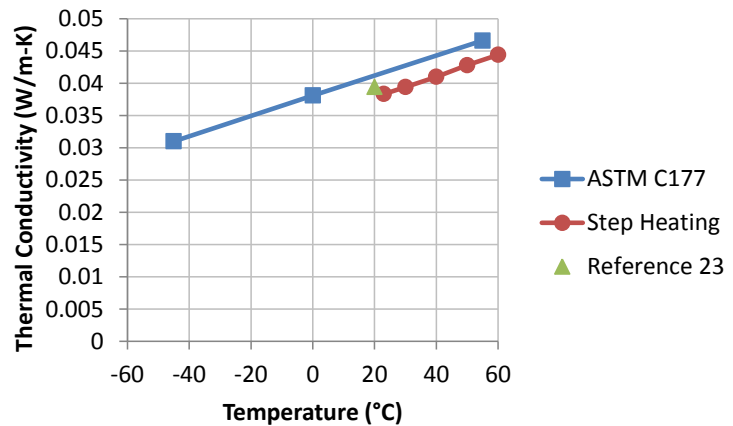


Figure 7. Thermal conductivity of Rohacell® at 760 torr (1 earth atmosphere) as a function of temperature.

measurements for the thermal conductivity of cork were not in as good agreement with each other and literature as the measurements for Rohacell® were. These results should be considered in light of this uncertainty, and used with the appropriate levels of caution. Finally, the thermal conductivity of numerous materials as a function of temperature is shown in Figure 9. To our knowledge, measurements of these materials have not previously been published.

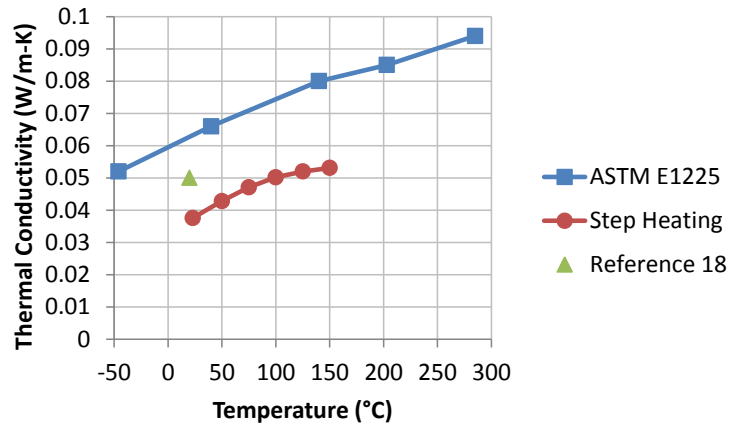


Figure 8. Thermal conductivity of cork at 760 torr (1 earth atmosphere) as a function of temperature.

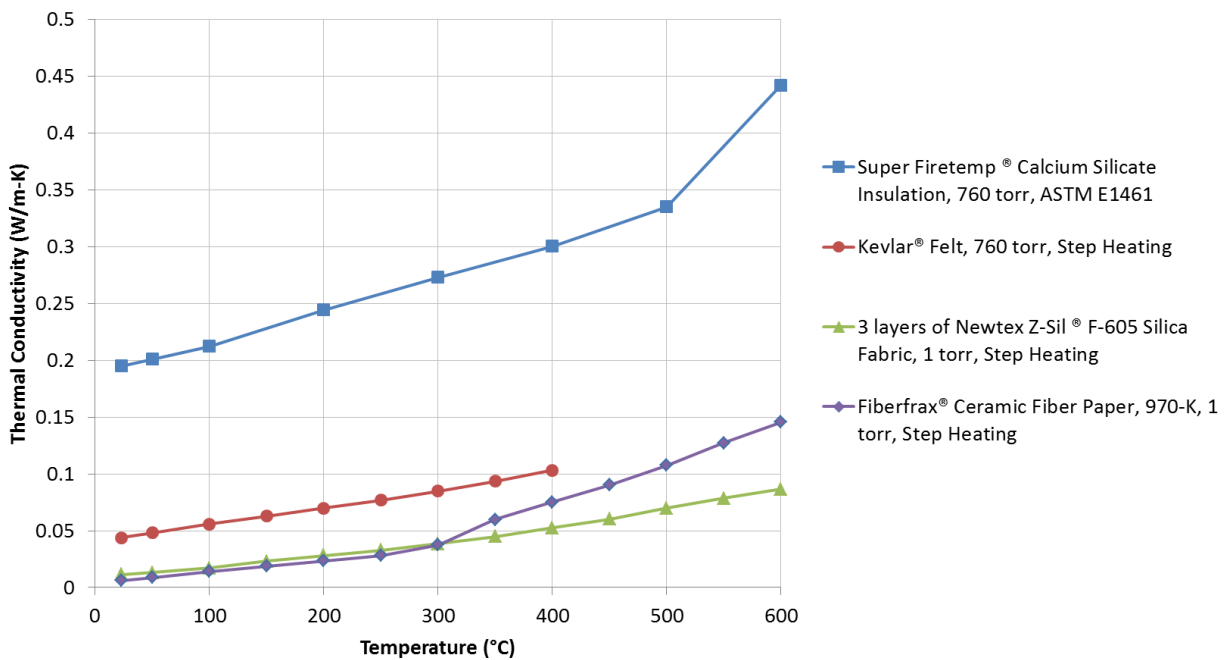


Figure 9. Thermal conductivity of numerous materials as a function of temperature.

Of all the thermal conductivity measurements presented in this section, one trend that stands out is that all of these materials have a thermal conductivity which increases as a function of temperature. In addition, the thermal conductivity of many materials is dependent on atmospheric pressure. These are well known trends of thermal insulators. Most thermal insulators have a large number of gaps, spaces, and voids in order to decrease their thermal conductivity, but it is interesting to note that thermal conduction is not the only phenomenon that occurs within thermal insulators. Rather, the parameter of thermal conductivity is used as the sole metric to describe insulators as a matter of convenience and simplicity. In reality, conduction, convection, and radiation all occur within the insulators. The radiative component of heat transfer increases as a strong function of absolute temperature, which leads to a higher measured thermal conductivity of materials at higher temperatures. The convective component of heat transfer increases as a function of absolute pressure and is not present in vacuum conditions, which leads to a higher measured thermal conductivity of materials at higher pressures. Another reason that higher pressure gasses may affect thermal conductivity is due to rarefied gas effects and the mean free path of gasses. Thankfully, it is not necessary to attempt numerical simulation or analysis of these more complex phenomena within the insulation itself, since the measured experimental thermal conductivity serves to combine all the phenomena into one convenient and simple metric which can be used for numerical calculations.

V. Conclusion

Numerous measurements of thermal emissivity, solar absorptivity, specific heat, and thermal conductivity were conducted over the course of the LDSD test vehicle development and presented in this paper. Some of these measurements were performed as a check on previously reported values, but some of the measurements were new and, to our knowledge, have not been previously reported. Many of these materials are low cost and are available for commercial off the shelf (COTS) purchase with typical applications in metal working, firefighting, and industrial processes. It is our hope that these material property measurements will be of use to others in the engineering community. If more details on the measurements are needed, additional information is available in the test reports generated over the course of this work²⁴⁻³¹.

Acknowledgments

The development described in this paper was carried out at the Jet Propulsion Laboratory, California Institute of Technology, under a contract with the National Aeronautics and Space Administration. The authors express their thanks to NASA's Office of the Chief Technologist for supporting this effort and enabling a select few to push the envelope. The authors wish to thank several of their colleagues who helped with these material property measurements: Sandria Grey, Brant Cook, John-Luke Wolff, Eric Oakes, Gabriel Molina, Christopher Tanner, and Kris Katagiri. The authors also wish to thank Bob Larsen at Thermophysical Properties Research Laboratory, Inc., Don Schneider at Precision Measurements and Instruments Corporation, and Bryan Kiep at AZ Technology for their assistance in performing material property measurements. Reference herein to any specific commercial product, process, or service by trade name, trademark, manufacturer, or otherwise, does not constitute or imply its endorsement by the United States Government or the Jet Propulsion Laboratory, California Institute of Technology. Copyright 2015 California Institute of Technology. Government sponsorship acknowledged.

References

- ¹Lundstrom, R.R., Raper, J.L., Bendura, R.J., and Shields, E.W., "Flight Tests of Viking Parachute System in Three Mach Number Regimes I: Vehicle Description, Test Operations, and Performance," NASA Technical Note TN D-7692, 1974.
- ²Bendura, R.J., Lundstrom, R.R., Renfro, P.G., and LeCroy, S.R., "Flight Tests of Viking Parachute System in Three Mach Number Regimes II - Parachute Test Results," NASA Technical Note TN D-7734, pp. 1-96, 1974.
- ³Raper, J.L., Michel, F.C., and Lundstrom, R.R., "The Viking Parachute Qualification Test Technique," in AIAA 4th Aerodynamic Decelerator Systems Conference, Palm Springs, CA, 1973.
- ⁴Smith, B.P., Tanner, C.L., Mahzari, M., Clark, I.G., Braun, R.D., and Cheatwood, F.M., "A Historical Review of Inflatable Aerodynamic Decelerator Technology Development," in IEEE Aerospace Conference, Big Sky, MT, 2010.
- ⁵Gallon, J.C., Clark, I.G., Rivellini, T.P., Adams, D.S., and Witkowski, A., "Low Density Supersonic Decelerator Parachute Decelerator System," in AIAA Aerodynamic Decelerator Systems Conference, Daytona Beach, FL, 2013.
- ⁶Giersch, L., Rivellini, T., Clark, I., Shook, L., Ware, J., and Welch, J., "SIAD-R: A Supersonic Inflatable Aerodynamic Decelerator for Robotic Missions to Mars," in AIAA Decelerator Systems Conference, Daytona Beach, FL, 2013.
- ⁷Coatta, D., Jurewicz, D., Tutt, B., Rivellini, T., Clark, I., "Development and Testing of an 8 Meter Isotensoid Supersonic Inflatable Aerodynamic Decelerator," in AIAA Aerodynamic Decelerator Systems Conference, Daytona Beach, FL, 2013.
- ⁸NASA, "Fact Sheet: Low Density Supersonic Decelerators," 26 March 2013. [Online]. Available: http://www.nasa.gov/pdf/737628main_Final_LDS_D_Fact_Sheet_3-26-13.pdf. [Accessed 20 January 2014].
- ⁹Cook, B.T., Blando, G., Kennett, A., Heydt, M.V., Wolff, J.L., and Yerdon, M., "High Altitude Supersonic Decelerator Test Vehicle," in AIAA Aerodynamic Decelerator Systems Conference, Daytona Beach, FL, 2013.
- ¹⁰Buna, T., and Battley, H.H., "Thermal Design and Performance of the Viking Balloon Launched Decelerator Test Vehicles," in AIAA/ASME Thermophysics and Heat Transfer Conference, Boston, MA, 1974.
- ¹¹Mastropietro, A.J., Pauken, M., Sunada, E., and Gray, S., "Thermal Design and Analysis of the Supersonic Flight Dynamics Test Vehicle for the Low Density Supersonic Decelerator Project," AIAA-2013-3348 in 43rd International Conference on Environmental Systems, Vail, CO, 2013.
- ¹²Redmond, M., Mastropietro, A.J., Pauken, M., and Mobley, B., "Passive Thermal Control for the Low Density Supersonic Decelerator (LDS) Test Vehicle Spin Motors Sub-System," ICES-2014-031 in 44th International Conference on Environmental Systems, Tuscon, AZ, 2014.
- ¹³Mastropietro, A.J., Kempenaar, J., Redmond, M., Pauken, M., and Ancarrow, W., "First Test Flight Thermal Performance of the Low Density Supersonic Decelerator (LDS) Supersonic Flight Dynamics Test (SFDT) Vehicle," ICES-2015-328 in 45th International Conference on Environmental Systems, Bellevue, WA, 2015.
- ¹⁴AZ Technology, "TESA 2000, Portable Emissometer/Reflectometer and Solar Reflectometer," [Online]. Available: <http://www.aztechnology.com/optical-instruments-tesa2000.html>. [Accessed 13 December 2014].
- ¹⁵Gilmore, G. (ed.), "Spacecraft Thermal Control Handbook," 2nd ed., The Aerospace Corporation, 2002.

- ¹⁶Henninger, J., "Solar Absorptance and Thermal Emittance of Some Common Spacecraft Thermal Control Coatings," NASA Reference Publication 1121, 1984.
- ¹⁷American Society for Testing and Materials, "ASTM E1269: Standard Test Method for Determining Specific Heat Capacity by Differential Scanning Calorimetry," ASTM International, West Conshohocken, PA, 2011.
- ¹⁸Incropera, F.P., and DeWitt, D.P., "Introduction to Heat Transfer," 3rd ed., John Wiley & Sons, 1996.
- ¹⁹DuPont, "Kevlar Aramid Fiber Technical Guide," [Online]. Available: <http://www.dupont.com/products-and-services/fabrics-fibers-nonwovens/fibers/articles/kevlar-properties.html>. [Accessed 19 January 2015].
- ²⁰Zircar Ceramics, "Alumina Mat," [Online]. Available: <http://www.zircarceramics.com/pages/flexible/specs/almat.htm>. [Accessed 19 January 2015].
- ²¹American Society for Testing and Materials, "ASTM C177: Standard Test Method for Steady-State Heat Flux Measurements and Thermal Transmission Properties by Means of the Guarded Hot Plate Apparatus," ASTM International, West Conshohocken, PA, 2013.
- ²²American Society for Testing and Materials, "ASTM E1461: Standard Test Method for Thermal Diffusivity by the Flash Method," ASTM International, West Conshohocken, PA, 2013.
- ²³Evonik Industries AG, "ROHACELL for the Automotive Industry," [Online]. Available: <http://www.rohacell.com/sites/dc/Downloadcenter/Evonik/Product/ROHACELL/product-information/ROHACELL%20Automotive.pdf>. [Accessed 23 January 2015].
- ²⁴Berry, D., Schneider, D., and Oakes, D., "Thermal Conductivity Measurements of Composite Sandwich Specimens," PMIC Job # 14312, 2013.
- ²⁵Berry, D., Schneider, D., and Oakes, D., "Thermal Conductivity Measurements of a Cork Specimen," PMIC Job # 14313, 2013.
- ²⁶Kiep, B., "Measurement Test Report," Job #M-48, 2013.
- ²⁷Larsen, R., "Thermophysical Properties of Kevlar Felt," TPRL Report #5134, 2013.
- ²⁸Larsen, R., "Thermophysical Properties of One Alumina Mat Sample," TPRL Report #5137, 2013.
- ²⁹Larsen, R., "Thermophysical Properties of Two Materials," (Cork and Rohacell) TPRL Report #5102, 2013.
- ³⁰Larsen, R., "Thermophysical Properties of Two Samples," (Z-Sil and Ceramic Fiber Paper) TPRL Report #5160, 2013.
- ³¹Larsen, R., and Trombley, K., "Thermophysical Properties of DCSM Material," TPRL Report #5188, 2014.